High-Performance and Low-Cost Macroporous Calcium Oxide Based Materials for Thermochemical Energy Storage in Concentrated Solar Power Plants.

Pedro E. Sánchez Jiménez[1,*], Antonio Perejón[2], Mónica Benítez Guerrero[1], José M. Valverde[3], Carlos Ortiz[3], Luis A. Pérez Maqueda[1].

[1] Instituto de Ciencia de Materiales de Sevilla, C.S.I.C.-Universidad de Sevilla, C. Américo Vespucio nº49, 41092 Sevilla, Spain.
[2] Departamento de Química Inorgánica, Facultad de Química, Universidad de Sevilla, Sevilla, Spain.
[3] Faculty of Physics, University of Seville, Avenida Reina Mercedes s/n, Sevilla, Spain.

Abstract

High energy density, cycling stability, low cost and scalability are the main features required for thermochemical energy storage systems to achieve a feasible integration in Concentrating Solar Power plants (CSP). While no system has been found to fully satisfy all these requirements, the reversible $CaO/CaCO_3$ carbonation reaction (CaL) is one of the most promising since CaO natural precursors are affordable and earth-abundant. However, CaO particles progressively deactivate due to sintering-induced morphological changes during repeated carbonation and calcinations cycles. In this work, we have prepared acicular calcium and magnesium acetate precursors using a simple, cost-effective and easily scalable technique that requires just the natural minerals and acetic acid, thereby avoiding expensive reactants and environmentally unfriendly solvents. Upon thermal decomposition, these precursors yield a stable porous structure comprised of well dispersed MgO nanoparticles coating the $CaO/CaCO_3$ grains that is resistant to pore-plugging and sintering while at the same time

* Corresponding authors: pedro.enrique@icmse.csic.es

exhibits high long term effective conversion. Process simulations show that the empoyment of these materials could significantly improve the overall CSP-CaL efficiency at the industrial level.

1. Introduction

The undeniable impact of greenhouse gas emissions on environment and climate is progressively encouraging governments and companies to promote renewable energy technologies in order to reduce anthropogenic CO_2 emissions [1, 2]. Electricity production by coal-fired power plants still accounts for a significant share of global warming emissions albeit it is sought to be steadily replaced by renewable sources of energy within the next decades. However, the current lack of large scale, low cost, efficient and environmentally friendly energy storage technologies curtails the replacement of fossil fuel based energy conversion technologies. The complex electricity grid that powers nowadays society requires a continuous matching of supply and demand, thereby making the intrinsic intermittency of solar and wind a critical challenge to overcome. Concentrated Solar Power (CSP) is a rapidly growing technology that offers the possibility of integrating energy provision with large scale thermal energy storage (TES) [3-6]. Basically, a CSP plant is composed of solar concentrators that focus sunlight on a receiver where a working fluid is heated up. Then, the fluid is transported to a steam turbine attached to a electrical generator. Current plants are constructed according to four configurations; parabolic trough collectors, solar parabolic dishes, linear Fresnel reflectors and solar power tower [4, 5]. Current commercial CSP plants with integrated TES allow transferring the heat generated by direct solar radiation to a high specific heat mixture of molten salts, most usually nitrates. This energy is stored in form of sensible heat and can be later used to generate electrical power on demand, thereby enabling the use of solar energy even after sunset [7, 8]. Nevertheless, molten salts competitiveness

against fossil fuel power plants is severely hindered by limited thermal stability, high freezing temperature, corrosion issues and high cost [9, 10]. Therefore, alternative CSP-TES systems based on solid particles able to function at high temperatures have been attracting increasing attention [11].

A rapidly growing alternative to TES is thermochemical energy storage (TCES), in which solar radiation is used to directly drive a reversible endothermic chemical reaction [12, 13]. The ensuing products are separately stored so that they can be brought back together to carry out the reverse exothermic reaction whenever power is required. TCES has inherently higher energy densities than TES since energy is stored as chemical potential in addition to latent or sensible heat. Moreover, the reaction by-products can be stored indefinitely in a stable form with negligible thermal losses [14]. Considering these advantages, TCES could well constitute the key for a widespread deployment of CSP technologies. TCES systems currently under investigation comprise metallic hydrides, organic and redox reactions, alkaline earth hydroxides, and several carbonates. Extensive reviews of the different available systems can be found in recent studies [13-15]. Among them, the cyclic reversible conversion between CaO and $CaCO_3$, also known as Calcium-Looping (CaL) process, stands out due to the high energy density achievable (theoretically about 3.2 GJ/m^3 as compared to 0.8 GJ/m^3 stored by solar salts as sensible heat), the low cost (∼10 €/ton) and ample availability of natural CaO precursors, mainly limestone and dolomite [14, 16]. Moreover, the high reaction temperatures allows for efficient power generation cycles. The environmental and economic advantages of the $CaO/CaCO_3$ system over the use of molten salts have been summarised in recent studies [17, 18].

Even though the proposal of CaL for TCES dates back to the 1970s [19, 20], the as then unsolved significant reactivity drop of CaO during repeated cycles made the interest decline. However, the quickly developing potential of CaL for capturing CO_2 in coal fired power plants (CaL-CCS) has again attracted the attention of researchers on the CaL process [21, 22].

3

The rapid decay in reactivity displayed by CaO as the number of cycles increase has been generally attributed to significant sintering and crystallization during the calcination stage. Moreover, grain growth and sintering is strongly promoted by the presence of CO_2 in the reaction environment [23-25]. Several avenues have been pursued to attenuate sorbent deactivation, such as thermal and mechanical pretreatments [26, 27], the employment of alternative calcium based minerals [16, 28] or even synthetic sorbents [29, 30]. The most promising results has been obtained by including inert additives that provide structural stability [31, 32] or by engineering the sorbent morphology so as to increase the fraction of CaO active for CO_2 capture [33, 34]. Despite important advances, the harsh operation conditions in the CaL-CCS process (carbonation carried out at 650 ºC under 15% v/v CO_2 concentration and calcination under 70-90% v/v CO_2 concentration at high temperatures of ~950 °C) still results in too low residual conversions for feasible TCES applications [35, 36]. Nevertheless, it has been observed that carrying out the carbonation reaction at high temperature and high CO_2 concentration entails a beneficial effect in subsequent carbonation stages provided intermediate calcinations are done in inert gas atmosphere in order to prevent the extensive sintering caused by CO_2 [37, 38]. While such working conditions are unrealistic for CaL-CCS, they could be applied in a potential integration with CSP aiming at energy storage. Thus, it has been recently shown that implementing a carbonation stage in pure CO_2 at about 850 ºC followed by a calcination stage in Helium at 725 ºC significantly reduces the deactivation, eventually leading to residual effective conversions about three times higher than in achieved in conventional CaL-CCS conditions [39]. Taking these findings into account, a CSP-CaL integration scheme has been recently proposed [40, 41]. The high thermal conductivity and extremely favourable CO_2 diffusivity of Helium is exploited in order to further reduce the temperature required for full calcination in short residence times, thereby allowing the use of less expensive solar receivers. At the same time, lower temperatures would also benefit the efficiency by reducing radiative losses [42, 43]. Since Helium is an

expensive gas, a closed cycle is needed in order to avoid the need of a continuous feed. Out of the four different solar plant configurations, the tower technology is the most suitable for the CaL system due to the high temperatures needed required for fast $CaCO_3$ decomposition. Such high temperatures could be attained by solar particle receivers [44]. Recent proposals of solar calciner reactors has been reviewed in [45, 46], some of which are been experimentaly tested up to 50 kW [47].

However, despite much improved cyclic stability, reported CaO conversions are still far from the theoretical maximum due to pore plugging. This phenomenon is caused by the rapid formation of a 50 to 100 nm thickness layer of $CaCO_3$ on the surface of the CaO particles that curtail further CO_2 diffusion into the porous unreacted particle core [48, 49]. This detrimental effect is more pronounced the larger the particle size and consequently, suitably high conversions are only obtained for small particles which are largely unpractical for use in large scale plants [48].

A solution to avoid or minimize pore plugging would be the design of sorbents with an stable pore structure in order to secure accessibility of calcium to CO_2 despite repeated cycling. Highly porous Ca-based structures, such as the multi-shelled $CaO-Al_2O_3$ microspheres recently reported [33] illustrate the critical importance of free pore volume for CO_2 sequestration performance [50, 51]. However, lab-scale preparation methods such as self-assembly or CVD are too costly and therefore unsuitable for large scale systems. In this work, we have devised a simple, cost-effective and scalable strategy to prepare $CaCO_3$ and $CaCO_3$-MgO composites using calcium and magnesium acetate precursors prepared from natural limestone and dolomite. While previous studies had shown that CaO coming from acetate precursors was composed of small particles exhibiting slightly enhanced conversion, such morphology also entailed a rapid deterioration in the conversion along consecutive carbonation and calcinations cycles due to the higher sinterability [52]. In this work, the acetate precursors have been prepared in acicular shape which upon decomposition leads to

5

the formation of an open carbonate structure remarkably resistant to sintering that is capable of maintaining a high CaO reactivity along a large number of calcinations/carbonation (calc/carb) cycles. Concerns due to the increased cost of calcium magnesium acetates (CMA) over natural minerals can be mitigated by the feasibility of producing acetic acid from industrial waste or bio-oils, which reduces the cost of CMA to about one third as compared to analytically pure CMA [53, 54]. Our study is supported with a detailed SEM analysis of the textural changes undergone by the materials during repeated carb/calc cycles aiming at identifying the underlying deactivation mechanism. Moreover, multicycle CaO conversion results have been used in process simulations to assess the enhancement of the overall CaL-CSP cycle efficiency at the industrial scale by using the CMA sorbents as compared to natural limestone.

2. Materials and Methods

2.1. Materials

Natural limestone received from Matagallar quarry (Pedrera, Spain) and natural dolomite from Bueres quarry (Asturias, Spain) are employed in this work. The limestone employed has a purity of 99.6 wt. % $CaCO_3$ whereas the dolomite has $CaMg(CO_3)_2$ as the main phase (94.4 wt. %), with the rest being $CaCO_3$ (~5%) plus impurities (<1%). Acetic acid (99.9%) purchased from VWR Chemicals (CAS: 64-19-7) was used to prepare the acetates.

2.2. Characterization Methods

Carbonation/calcination cycles were carried out using a thermogravimetric analyzer (TGA) Q5000IR from TA Instruments. CaL-CSP multicycle tests consisted of 5-minute calcination stages at 725 °C in Helium and 5-minute carbonation stages in pure CO_2 atmosphere at 850 °C. In order to avoid undesired heat and mass transfer effects, small masses of about

20 mg were used in each test so that about 10 mg of calcium carbonate is obtained after acetate thermal decomposition. Fast transitions (300 °C/min) between stages were implemented to mimic realistic conditions.

Scanning Electron Microscopy (SEM) micrographs were taken using an ultra-high resolution HITACHI S4800 instrument. X-ray diffractograms were acquired in the 2θ range from 5° to 90° using a XRD data were collected on a Rigaku Miniflex diffractometer working at 45 kV and 40 mA.

Particle size distributions (PSDs) were measured by laser diffraction analysis using a Mastersizer 2000 equipment (Malvern). For this purpose, the samples were previously dispersed in 2-propanol and sonicated for 30 s to loosen particle aggregates.

Nitrogen adsorption–desorption isotherms were measured at 77 K (-196 °C) by employing a ASAP2420 (Micromeritics) instrument. Prior to the analysis, the samples were degassed at 250 °C for 3 h. Total surface areas (S_{BET}) were determined using the BET equation. Since surface area analysis require a relatively large amount of sample, calcinations experiments were also carried out in a tubular furnace in order to obtain samples in enough quantity. Thus, 500 mg samples were calcined in N_2 for 20 min at 750 °C. Heating and cooling ramps were performed at 10 °C/min.

2.3. Synthesis of Calcium Acetate and Calcium Magnesium Acetate precursors.

Limestone and dolomite samples were first calcined in a furnace at 900 °C for 2 h under air to produce the calcium and magnesium oxides, which were subsequently treated with diluted acetic acid (50% volume in aqueous solution). The mixture was kept at room temperature for 24 h under stirring. Then, the solution was heated and dried at 60 °C to obtain the calcium acetate (CA) and calcium and magnesium acetate (CMA) crystals. The method can be found

in more detail in [55]. Three samples with different compositions have been prepared; CaAc using limestone as starting material, CaMgAc using dolomite, and finally CaMg50Ac from equal mass quantities of limestone and dolomite. X-ray diffraction patterns recorded (**Figures 1a to 1c**) show that CaAc is composed of hydrated CA while CaMgAc and CaMg50Ac consist of a mixture of hydrated CA and hydrated CMA in different ratios. Since CMA contains two atoms of magnesium per each atom of calcium, CaMgAc and CaMg50Ac are composed of a mixture of CA and CMA in different proportions. No other crystalline phases were detected. **Figure 1d** shows the thermogravimetric records corresponding to the calcination of the three acetate samples prepared. By measuring the mass losses involved in each consecutive step (dehydration, thermal decomposition of acetate and decarbonation) it is possible to quantify the actual Mg/Ca ratio present in each sample. Thus, CaMgAc contains a Mg/Ca ratio of 0.92 while CaMg50Ac is enrichened in calcium, reaching a Mg/Ca ratio of 0.34. SEM images in **Figure 1e** illustrate the typical acicular morphology of precipitated CA and CMA crystals, which will be critical for the subsequent material behavior under CaL cycles. Crystals are generally between 2 and 6 μm long. Particle size distributions (PSDs) were determined for all samples after the deacetylation process, in order to better compare them with other materials. PSDs are shown in **Figure 1f**, demonstrating relatively large average particle sizes, with d(50) values of 139 μm for CaAc, 220 μm for CaMgAc and 267 μm for CaMg50Ac.
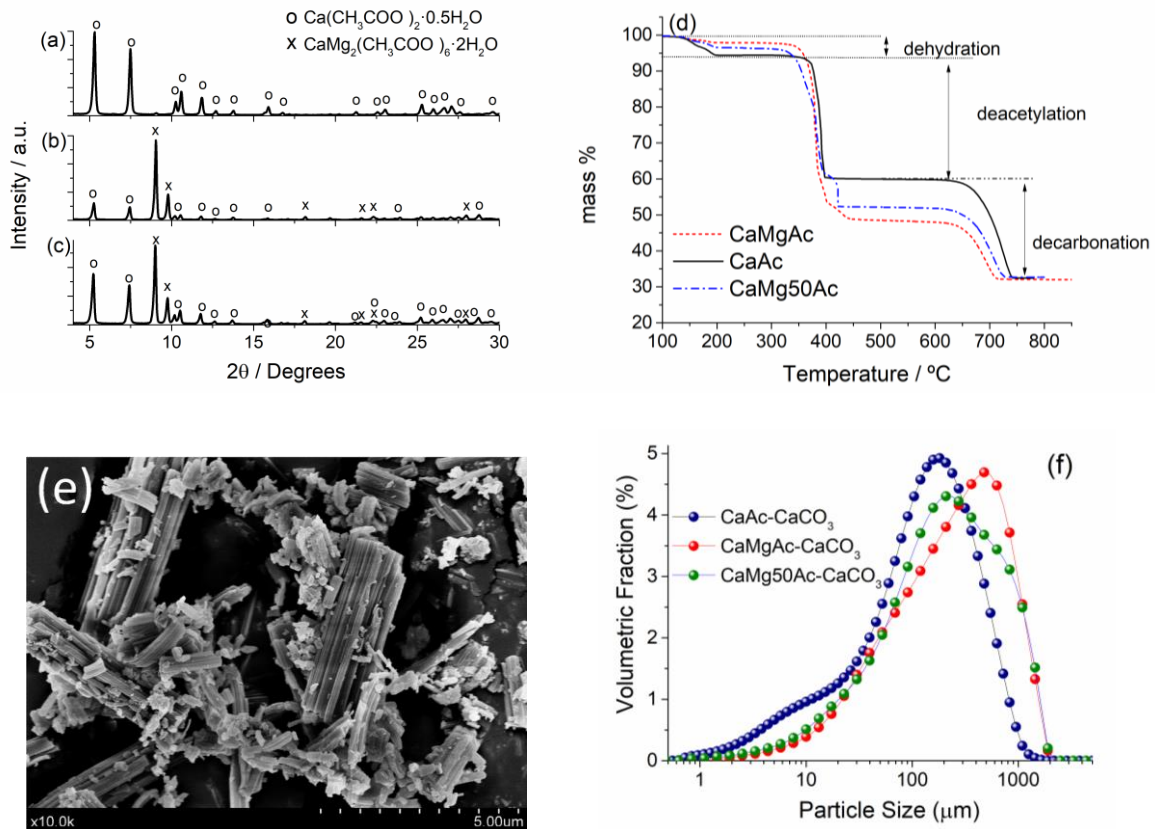
Figure 1. XRD diffractograms corresponding to the acetates formed from (a) limestone, (b) dolomite and (c) a 1:1 mass mixture of limestone and dolomite. (d) TGA curves recorded during thermal decomposition of acetate samples subjected to a heating rate of 10 ºC min^{-1} in air. (e) SEM micrographs of calcium acetate crystals. (f) Particle size distribution plots of the different samples after deacetylation.

3. Results and Discussion

3.1. Multicycle effective conversion in CaL-CSP conditions.

CaL-CSP multicycle tests were carried out by means of cyclic thermogravimetric experiments consisting of 5-minute calcination stages at 725 ºC in Helium followed by 5-minute carbonation stages in pure CO_2 atmosphere at 850 ºC. Fast transitions between stages were implemented to mimic realistic conditions.

9

Figure 2a shows, as an example, the complete multicycle thermogram recorded for the CaMgAc sample. Similar thermograms for CaAc and CaMg50Ac can be found in **Figure S5**. **Figure 2b** illustrates a detail of the sixth cycle where time evolution of mass can be clearly observed and the three carbonation, calcinations and transition stages are identified.
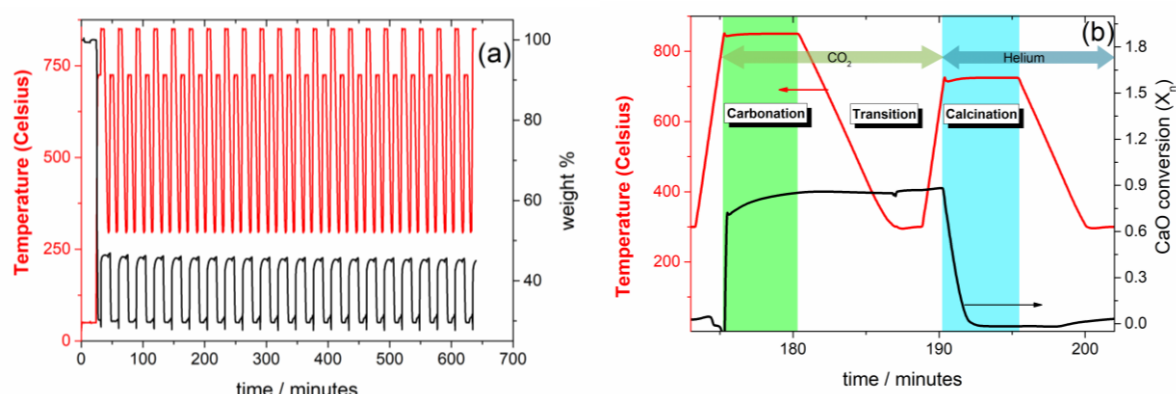
Figure 2. (a) Time evolution of temperature and sample mass of the CaMgAc sample along multicycle CaL tests (carbonation carried out at 850 °C in 100% CO_2 and calcination at 725 ºC in Helium). (b) Detail of the sample effective CaO conversion at the sixth carb/calc cycle. Shaded areas identify carbonation and calcinations segments and arrows indicate the type of reaction gas at each time.

The relevant parameter for evaluating the performance of a material under CaL-CSP tests is the energy released per unit mass of material entering the carbonator at any given cycle, which is calculated by the expression $\Delta H_r^0/W_{CaO}$ (kJ/g), where $\Delta H_r^0=-178$ kJ/mol is the reaction enthalpy. Thus, the mass of inert components has to be considered for an objective comparison. For this purpose, the effective conversion parameter, $X_{ef,N}$, is defined as the ratio of the CaO mass converted in the carbonation stage of each cycle to the total sample mass before carbonation, including inert compounds whenever present. **Figure 3** shows a comparison of the multicycle effective conversion measured for the three samples tested;

10

CaAc, CaMgAc and CaMg50Ac, as well as for raw limestone and dolomite minerals. **Figure 3a** clearly illustrates the critical role that particle size plays on limestone performance; larger limestone particles (>45 μm) are reduced to one fifth of their potential conversion capability within a few cycles due to pore plugging [48]. While smaller limestone particles exhibit notably better uptake capability, their residual conversion still decays to values about 0.4 after 20 cycles. Moreover, these fine particles cannot be used in circulating fluidized bed reactors. In contrast, the CaAc sample outperforms limestone despite its much larger particle size, attaining conversion values slightly over 0.6 after 20 cycles. Thus, the nascent CaO stemming from the decomposition of CA must be either more reactive or more accessible to CO_2 molecules. Nonetheless, a decay trend is still noticeable. This is in agreement with preceding works in which CaO coming from acetate precursors showed slightly larger conversions albeit at the expense of a rapid deactivation due to intense sintering [52]. Nevertheless, the improvement in performance over limestone here observed is larger than in previously reported CaO derived acetate precursors. This could be attributed to the acicular morphology of CaAc samples, as it will be discussed in the next section. Additionally, in previous works the carbonation reaction was carried out at moderate temperatures of about 600 ºC [52, 56], which are less favourable for the subsequent carbonation reactions than higher temperatures, as shown by Sarrion et al [39].

Figure 3b shows the effect of MgO on CaO conversion. It has been proven that the presence of inert MgO nanoparticles provides structural stabilization that serves to prevent pore plugging and minimizes the influence of particle size [48, 57]. Yet, such an stable conversion is only maintained for about 10 carb/calc cycles since MgO nanoparticles eventually segregate, thereupon losing their beneficial effect [39]. In terms of conversion, CaMgAc behaves similarly to dolomite yet without enduring the sudden decay triggered after 10 cycles. Thus, the CaO-MgO composite material formed after the acetate precursor decomposition

11

exhibits improved stability. Nevertheless, the maximum effective conversion achievable with these samples is limited due to the large amount of inert MgO present. Actually, CaMgAc performance is already near the theoretical maximum value of 0.61 (calculated according to the Mg/Ca ratio present in CaMgAc). Despite their stabilizing role, the inclusion of a large amount of inactive additive to carbonation reduces the effective conversion theoretically attainable at each cycle. Therefore, sample CaMg50Ac was designed to be enriched in CaO active for carbonation, containing about 75% Ca and 25% Mg in molar ratios. According to Figure 3b, the improvement in performance of this CaO enriched sample is notable; the effective conversion rises up to 0.7 without significant loss of cycling stability up to 30 cycles. The maximum theoretical effective conversion for this sample would be 0.80 taking into account the Mg/Ca ratio in the composite. This constitutes a truly outstanding performance since the reduction in the fraction of inert additives appears to greatly enhance the effective conversion without significant worsening in stability.

Figure 3c translates the effective conversion values into CaO conversion (X_{CaO}); this parameter indicates the fraction of calcium oxide that actually reacts in each carbonation phase with respect to the total available amount of CaO in the sorbent. Obviously, there is no distinction between effective conversion and calcium conversion in CaAc and limestone, both lacking inert additives. Regarding the samples with MgO, the larger the inert fraction the higher the resulting CaO conversions. Arguably, MgO nanoparticles not only act as a thermally stable support, but also substantially improve CaO availability for reaction with CO_2 given the high CaO conversions attained. The remarkable cycling stability of acetate derived samples is clearly demonstrated in Figure 3c as compared to the performance of natural minerals.
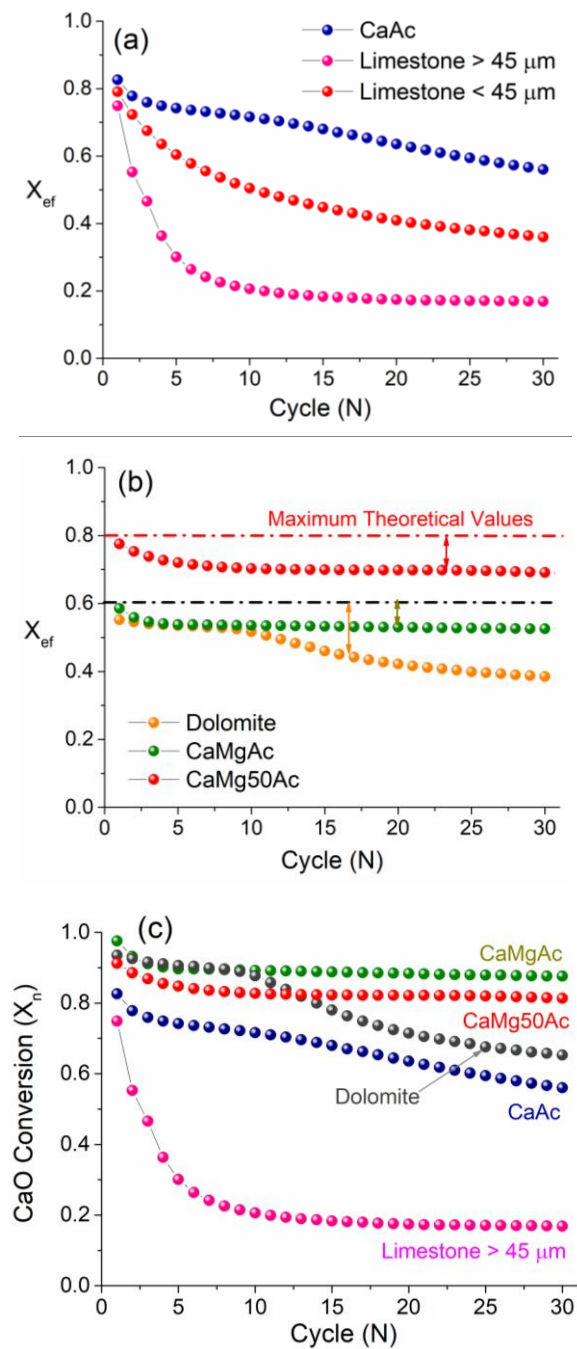
Figure 3. (a) and (b) effective conversion values, $X_{ef,N}$, as a function of the carb/calc cycles number, for natural limestone, dolomite, CaAc, CaMgAc and CaMg50Ac materials; (c) Multicycle CaO conversion (X_{CaO}). Maximum theoretical conversions are marked with dotted lines in (b).

3.2. Morphology changes during the reversible calcination/carbonation loops

The multicycle performance in the CaL process is intimately related to the materials morphology and microstructure evolution along the consecutive calcination/carbonation cycles. Thus, in order to elucidate the mechanisms that confer acetate derived CaO their remarkable multicycle performance, a detailed SEM analysis has been carried out in order to follow the morphological transformations undergone by the CaAc and CaMgAc samples along the different stages in the CaL process. SEM analysis of limestone has been also performed for comparison.

As it has been amply reported, CaO carbonation occurs in two well differentiated stages [58, 59]; an initial fast reaction-controlled phase that occurs on the surface of the particles followed by a solid-state diffusion-controlled phase driven by the counter-current diffusion of CO_3^{2-} and O^{2-} ions through the $CaCO_3$ product layer built upon the surface of the particles [60]. The latter diffusion controlled stage is characterized by considerably slower kinetics and becomes the rate-limiting step once the $CaCO_3$ product layer reaches a critical thickness of 50-100 nm [49]. In addition, it has been observed that the extent and kinetics of the diffusion controlled carbonation stage depends on several parameters; for instance, it is substantially promoted when calcination is performed under a high CO_2 concentration environment [59], by the inclusion of additives [50] or by modifying sample crystallinity by mechanical pretreatments [57]. On the other hand, when calcination is carried out at lower temperatures (725 ºC) in absence of CO_2, as in the multicycle CaL-CSP experiments here performed, the subsequent carbonation reaction takes place mostly during the initial reaction controlled phase, with a negligible contribution of the diffusion-controlled phase (Figure 2b). Carbonation kinetics in the fast reaction controlled phase is further promoted by the high temperature and CO_2-rich environment [61]. As a consequence, there is a rapid growth of a

14

plugging carbonate layer which prevents CO_2 from reaching the unreacted CaO underneath the blocking shell [58, 62].

The SEM images in **Figures 4a** and **4b** illustrate the morphology of $CaCO_3$ and $CaCO_3$-MgO composites arising from the deacetylation of the initial CaAc and CaMgAc samples (referred to as carbCaAc and carbCaMgAc, respectively). As it may be seen, an open structure composed of hierarchically aggregated flakes is formed. Small flakes aggregate in superior structures resembling the original acicular morphology of the acetates. This laminar morphology confers the carbonates stemming from the decomposition of the acetates a larger surface area as compared to raw limestone particles, which normally consists of compact aggregates of large grains (**Figure S6**). **Figures 4c and 4d** show SEM micrographs corresponding to the CaO and CaO-MgO composites resulting from the thermal decomposition of $CaCO_3$ in the carbCaAc and carbCaMgAc samples. As it can be observed, the laminar morphology of the preceding carbonates is preserved, which eventually proves key for the superior performance measured during ensuing calc/carb cycles. The initially large and smooth $CaCO_3$ flakes transform into aggregates of small ~50 nm spherical CaO grains, granting the CO_2 molecules ample accessibility to the entire volume of the material, hence the high CaO conversion achieved in the first cycles. The presence of Mg in the starting acetates not only promotes the porosity of the $CaCO_3$-MgO composite arising from the thermal decomposition but also grants the subsequent CaO-MgO produced after calcination the same macroporous, high surface area morphology. MgO is highly resistant to grain growth and sintering. It can be observed as small nanoparticles deposited onto $CaCO_3$ flakes or CaO grains even after a large number of calc/carb cycles. Again, this open porosity strongly favours a rapid, almost complete recarbonation as proven by the high CaO conversion shown in Figure 3c. This insight is important since gaining a deeper understanding of the

15

stabilization mechanism induced by the inclusion of additives would allow minimizing the load of inert material required.

While not as high as it occurs in acetate derived samples, CaO formed after calcination of large limestone particles also displays a notable initial CaO conversion of about 0.75 as compared to 0.82 in CaO derived from CaAc. As **Figure S7** shows, limestone derived CaO exhibits an extensively cracked surface as a consequence of the rapid CO_2 release from the interior of the particles, what grants a significant surface area available for carbonation. It is worthwhile to highlight the shape-memory feature displayed by CaO as the morphology of the preceeding carbonate, composed of large aggregated crystals, is roughly preserved. The substantial morphological differences between acetate derived and limestone derived CaO can be attributed to the different molar volume of reactants and products (36.9 cm^3/mol for $CaCO_3$, as compared to 16.7 cm^3/mol for CaO). Given that there is no noticeable change in the average limestone particle size after calcining nor in the particle shape, internal pore volume must be created to accomodate such large volumetric changes.
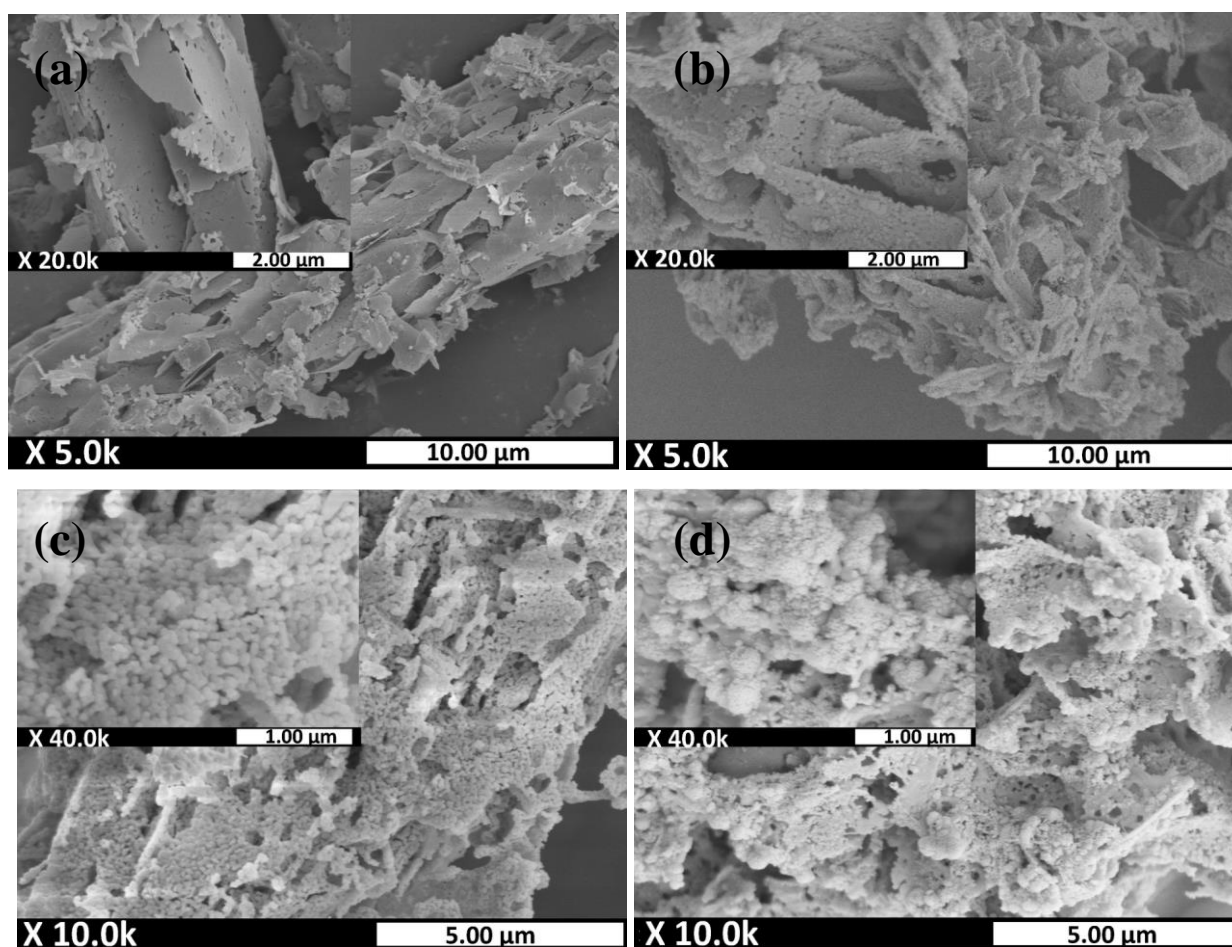
Figure 4: SEM images of (a) CaAc sample and (b) CaMgAc sample after the deacetylation stage, and of (c) CaAc and (b) CaMgAc after complete calcination at 850 ℃.

SEM micrographs in **Figure 5** show the divergent morphology adopted by the different samples studied after just one carbonation stage. Nascent $CaCO_3$ resulting from carbonation of limestone derived CaO presents a fully sintered surface, albeit a slightly more porous core is evidenced underneath (**Figure 5a**). On the other hand, the carbonation of the nanostructured CaO derived from acetate precursors leads to the formation of a significantly less dense structure, even though the grain size is approximately the same in both cases (**Figure 5b**). This is due to its notably different textural properties, with low density and large pore volume

that provides ample free space to accommodate both the volume increase and the grain growth. Finally, **Figure 5c** shows the morphology of the MgO containing sample (CaMgAc) is composed of $CaCO_3$ grains spaced apart by small MgO nanoparticles, which are responsible for hampering particle sintering.
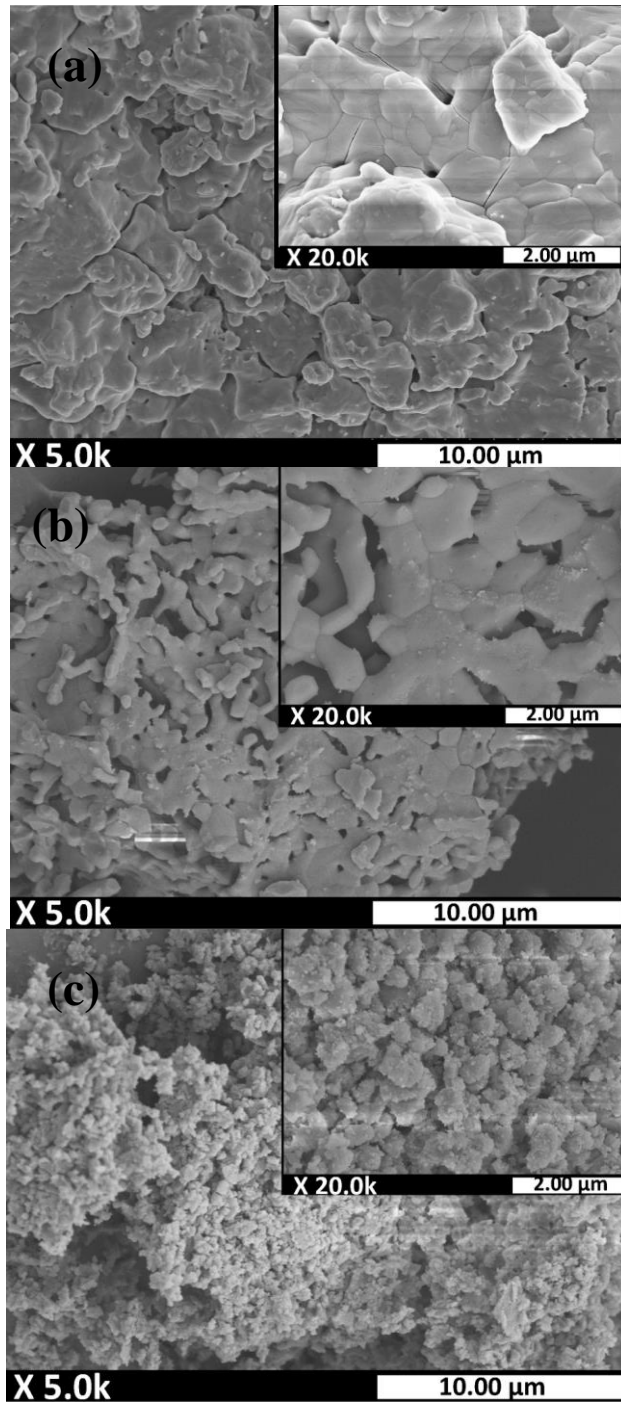
Figure 5. SEM micrographs comparing the morphology of $CaCO_3$ formed after the first carbonation stage in (a) limestone, (b) CaAc and (c) CaMgAc samples.

After repeated calc/carb cycles, these morphologies slowly evolve, eventually leading to sintering and pore closure in the case of raw limestone and CaAc samples, as portrayed in **Figure 6a** and **Figure 6b,** respectively. In both cases a considerably denser $CaCO_3$ microstructure rises after 30 carbonation stages. Limestone particles lead to a morphology in which the surface appears completely covered by a fairly dense mosaic-like surface composed of large $CaCO_3$ grains. The inset in Figure 6a shows in detail a fracture, revealing the significantly less sintered particle interior. This serves to demonstrate the pore-plugging effect in which only the surface of the particles undergoes repeated carbonation and calcinations reactions. Contrarily, while noticeably sintered, in the CaAc sample a number of large pores still remain. Also, there is no marked contrast between particle surface and interior. The homogenenity of the sample implies that a larger fraction of the particle has endured the calc/carb cycles, as it is otherwise expected by the consistently higher CaO conversion. The SEM image in **Figure 6c** corresponds to the CaMgAc sample after 30 carbonation stages. Again, the role of MgO in preserving cycling stability is highlighted [28, 48]. MgO nanoparticles form clusters covering the much larger $CaCO_3$ particles, hampering aggregation and sintering. SEM images in **Figures 6d, 6e** and **6f** shows the distinct morphology of the CaO derived from limestone, CaAc and CaMgAc samples after 30 calcination stages. Limestone-derived CaO (Figure 6d) displays the same mosaic structure resembling the preceding $CaCO_3$ due to the shape-memory nature of the $CaCO_3$ to CaO transformation. Thus, CaO particles present a low porosity surface which is easily plugged during carbonation, resulting in the rapid drop of the effective CaO conversion to very low values after a few carbonation/calcination cycles. In contrast, a globular structure with still substantial porosity is produced in the CaAc sample (Figure 6e). Therefore, it could be argued that the initially formed macroporous texture (Figure 4b) is more resilient to pore-plugging and sintering, hence retaining a notable residual effective capacity. Yet, the sintering of the material is noticeable, which leads to the progressive decline in CaO conversion discussed in Figure 3.

Finally, as shown in Figure 6f, CaO grains in CaMgAc sample undergoes no substantial grain growth even after 30 calcination stages, thereby retaining the overall macroporous structure unchanged since the first cycle. The sequence of SEM images here presented clearly justifies the distinct conversion profiles exhibited by the samples studied. Considering their different morphologies, it could be argued that the extension of the carbonation phase is proportional to the amount of CaO directly accessible to CO_2. When the exposed surface is decreased due to sintering, the CaO conversion is correspondingly reduced. Here it is shown that the inclusion of MgO coming from starting acetates helps preserving a high surface area available for reaction regardless of repeated cycling. This constitutes an important finding since so far the tested additives, even the MgO in natural dolomite, has always exhibited an unavoidable tendency to segregate with the number of cycles, thereby losing its stabilizing effect [28, 57].
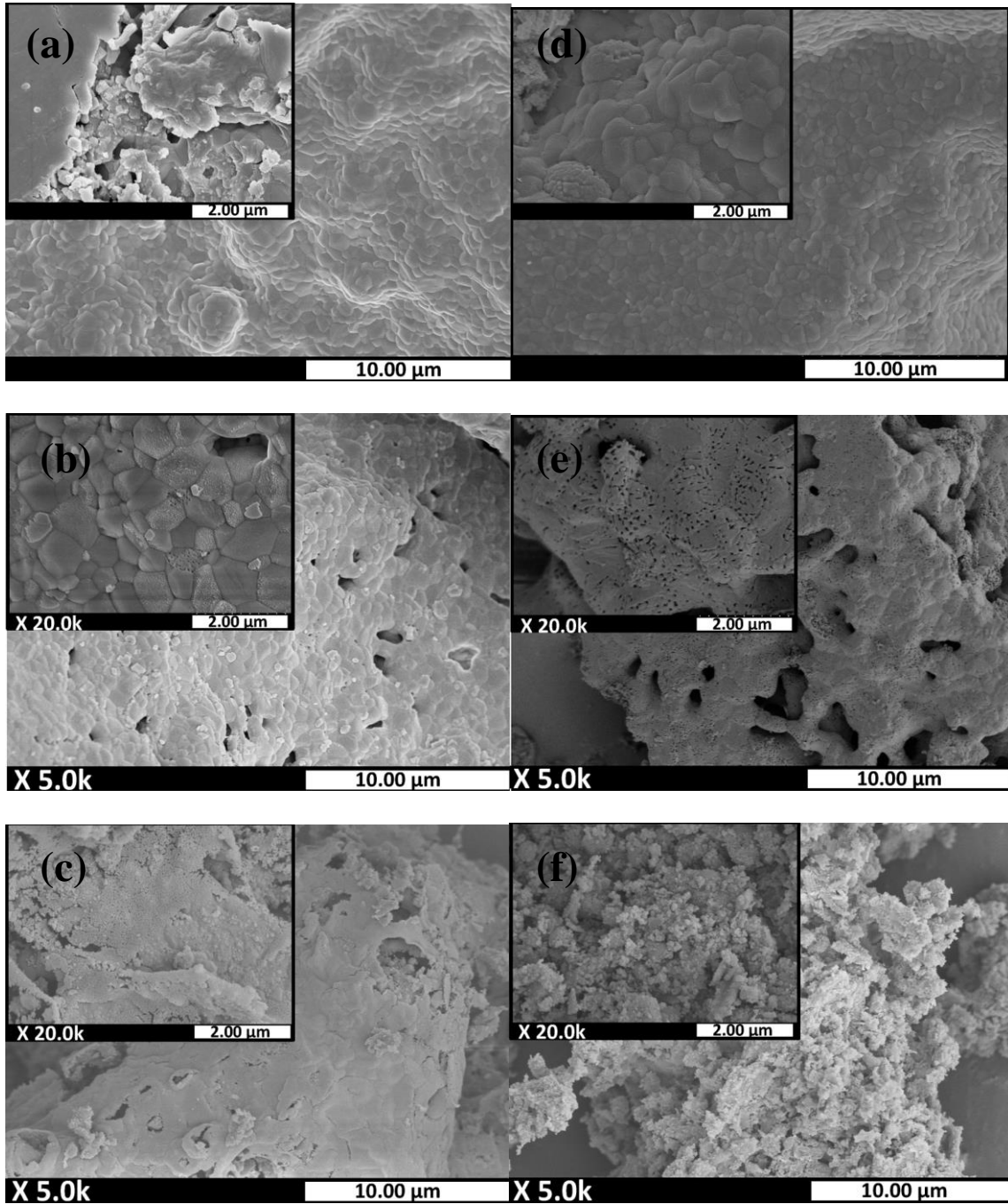
Figure 6. SEM micrographs comparing the morphology exhibited by the different tested samples in $CaCO_3$ form after 30 calc/carb cycles. (a) limestone, (b) CaAc and (c) CaMgAc. Also, it is shown the morphologies of the CaO stemming from the subsequent calcination of previous samples (d) limestone, (e) CaAc and (f) CaMgAc.

3.3. Implications for the efficiency of the CSP-CaL integration

This section highlights the impact that the enhanced performance of these acetate sorbents would have on the overall performance CSP-CaL. The CSP-CaL configuration proposed in the present work is based on the scheme proposed in [43] and the specific calc/carb conditions tested in previous sections. The CSP-CaL plant works as follow: concentrating solar power is used to preheat the streams entering the calciner and to carry out the calcination reaction. Full calcination occurs under Helium atmosphere which allows reducing the calcination temperature to 725ºC in short residence times (5 minutes) to simulate conditions as tested in Section 3.1 [39]. Note that the proposed scheme (Figure S8) is a closed cycle so it does not require the plant to be continuously fed by any gas stream [43]. This is especially relevant in the case of helium, which is an expensive gas. Once calcination takes place, the CaO is stored at about 700 ºC while the He-CO_2 stream is ideally separated through a membrane-based system [63]. After separation, the He stream is recirculated into the calciner while the pure CO_2 stream is passed through a heat recovery steam generator (HRSG) to use its high temperature as a previous step to be stored or used in the power cycle. To reduce the storage volume, the CO_2 to be stored is compressed up to 75 bar [40]. When energy provision is needed, the CaO is sent to the carbonator where reacts at 850ºC and atmospheric pressure (as tested in Section 3.1) with the CO_2 stream coming either from storage or the calciner side. The CO_2 entering the carbonator is well above the stoichiometric amount needed for carbonation. Thus, the CO_2 in excess that exits the carbonator acts as heat carrier to produce electrical power by means of a CO_2 closed regenerative Brayton cycle [40]. A detailed CSP-CaL integration scheme is shown in **Figure S8**.

This process has been modeled using the commercial software ASPEN PLUS™, assuming limestone, CaMgAc and CaMg50Ac as CaO precursor as well as the CaO conversion values

estimated in Section 3.1 The CSP-CaL plant is configured as a completely closed system, without make-up of fresh material to reduce the deactivation effect. Thus, a residual value of CaO conversion is reached after a long number of cycles. This residual CaO conversion is calculated by fitting the curves showed in Figure 3c as shown in Table S5. As a result, **Figure 7** shows the overall plant efficiency of the CSP-CaL plant for each of the CaO precursors considered. A detailed description of the assumptions considered in the modeling can be found in [41] whereas the detailed energy balance for each case is presented in Table S4. Moreover, a description about how the overall plant efficiency is calculated is shown in the supplementary material (section 5). For reasons of simplicity, ideal He/CO_2 separation has been assumed. Although it is out of the scope of the present work, an additional analysis would be required to account for the losses in both thermal and mechanical efficiency due to the gas separation process. Nevertheless, any correction coefficient would apply equally regardless the sorbent considered.
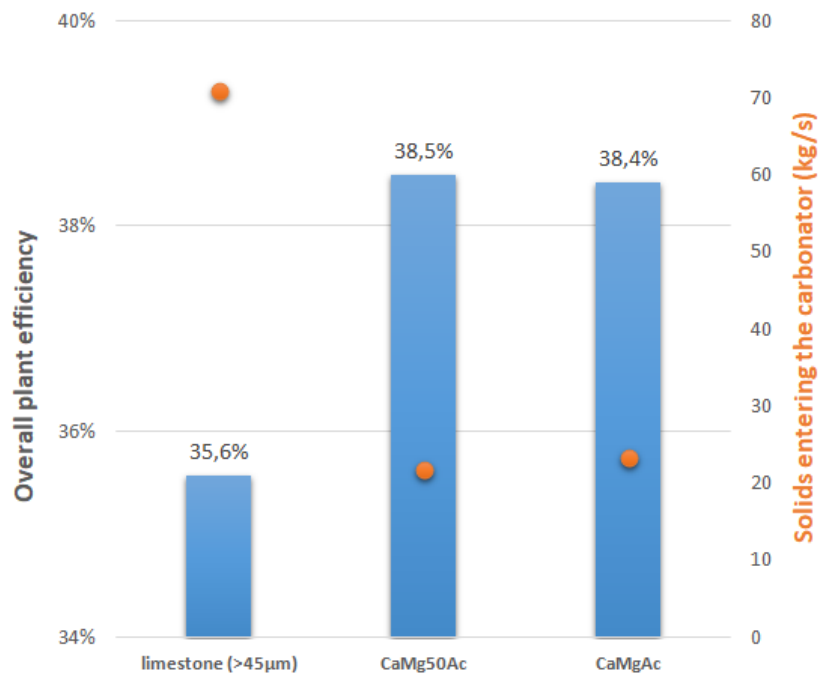
Figure 7. Overall plant efficiency of the CSP-CaL plant for each of the CaO precursors considered

The efficiency of the CaL-CSP strongly depends on CaO conversion. As it can be seen in Figure 7, the use of Calcium-Magnesium Acetates entails an overall efficiency about 3% points higher than in the case of limestone. This is mainly caused by a lower amount of solids being recirculated along the plant due to the higher multicycle CaO conversion achieved by CMA (as showed in Section 3.1). This is important since a high CaO conversion implies a lower amount of non-reactive CaO in the plant, which involves not only a reduction in the energy used to solids conveying but also a lower size of storage vessel, a lower size of heat exchangers and an improved use of the energy released in the carbonator [40] In spite of that, CaMgAc present a higher value of residual CaO conversion as compared to CaMg50Ac (X=0.88 against X=0.81). In the latter case the overall efficiency is deduced because of the higher amount of inert MgO recirculating along the plant. The high overall efficiency reached by using CaMgAc or CaMg50Ac could possibly be further increased by optimizing the CSP-CaL conditions, specially by increasing the PR and the carbonator temperature, which would lead to overall efficiencies around 41-44% [41]. Note that overall plant efficiency is

calculated as the ratio of net electrical production to net thermal input entering the calciner (without considering solar receiver efficiency). Finally, the large average particle size achieved by selecting CAM as CaO precursor, over 100 μm, facilitates the operation allowing use of commercial technology as CFB reactors.

4. Conclusion

The integration of the Calcium Looping process for thermochemical energy storage in Concentrated Solar power Plants is expected to reduce of electricity production costs and enhance dispatchability. The main drawbacks of the reversible reaction between $CaCO_3$ and CaO for this purpose are the limited conversion and poor cycling stability achieved by natural limestone particles. In order to mitigate the sintering induced CaO conversion decay, a material must possess high pore volume and surface area and preserve it along a large number of calc/carb cycles. In this work, we have demonstrated that such properties can be attained by using calcium and magnesium acetate as CaO precursors in a simple, cost effective and scalable method that requires just the natural minerals and acetic acid. Calcium acetate and calcium magnesium acetate crystallize as elongated fibers, yielding plate-like structures composed of CaO nanoparticles after calcination. Such morphology exhibits substantial porosity and can accommodate the volume changes accompanying the reversible reaction from $CaCO_3$ to CaO. Moreover, the inclusion of MgO nanoparticles stabilizes the highly porous structure against sintering. A remarkable CaO conversion value of about 0.7 is achieved and maintained even after 30 calc/carb cycles as compared to 0.15 as residual conversion of natural limestone. Moreover, contrary to other synthesis methods recently proposed to prepare high performance CaO sorbents, the precipitation method here reported does not require the use of complex equipment, expensive reactants or environmentally

26

unfriendly solvents. Therefore, its low cost would allow these CaO materials to be actually employed in real applications. Additionally, the relatively large particle size of these materials also constitutes an important advantage since it makes them suitable to large scale utilization in fluidised bed reactors. The utilization of calcium magnesium acetate as CaO precursor instead of limestone would increase the process overall efficiency about 3% over conventional limestone according to process simulations.

Acknowledgments

References

1. *World energy outlook*. 2017, International energy agency. www.iea.org/media/weowebsite/2017.
2. Betts, R.A., C.D. Jones, J.R. Knight, R.F. Keeling, and J.J. Kennedy, *El Niño and a record CO2 rise.* Nature Climate Change, 2016. **6**: p. 806, DOI: 10.1038/nclimate3063 https://www.nature.com/articles/nclimate3063#supplementary-information.
3. Lewis, N.S., *Research opportunities to advance solar energy utilization.* Science, 2016. **351**(6271), DOI: 10.1126/science.aad1920.
4. Liu, M., N.H. Steven Tay, S. Bell, M. Belusko, R. Jacob, G. Will, W. Saman, and F. Bruno, *Review on concentrating solar power plants and new developments in high temperature thermal energy storage technologies.* Renewable and Sustainable Energy Reviews, 2016. **53**: p. 1411-1432, DOI: 10.1016/j.rser.2015.09.026.
5. Weinstein, L.A., J. Loomis, B. Bhatia, D.M. Bierman, E.N. Wang, and G. Chen, *Concentrating Solar Power.* Chemical Reviews, 2015. **115**(23): p. 12797-12838, DOI: 10.1021/acs.chemrev.5b00397.

6.   Pelay, U., L. Luo, Y. Fan, D. Stitou, and M. Rood, *Thermal energy storage systems for concentrated solar power plants.* Renewable and Sustainable Energy Reviews, 2017. **79**: p. 82-100, DOI: 10.1016/j.rser.2017.03.139.

7.   Siva Reddy, V., S.C. Kaushik, K.R. Ranjan, and S.K. Tyagi, *State-of-the-art of solar thermal power plants—A review.* Renewable and Sustainable Energy Reviews, 2013. **27**(Supplement C): p. 258-273, DOI: https://doi.org/10.1016/j.rser.2013.06.037.

8.   Kuravi, S., J. Trahan, D.Y. Goswami, M.M. Rahman, and E.K. Stefanakos, *Thermal energy storage technologies and systems for concentrating solar power plants.* Progress in Energy and Combustion Science, 2013. **39**(4): p. 285-319, DOI: https://doi.org/10.1016/j.pecs.2013.02.001.

9.   Bauer, T., N. Pfleger, N. Breidenbach, M. Eck, D. Laing, and S. Kaesche, *Material aspects of Solar Salt for sensible heat storage.* Applied Energy, 2013. **111**(Supplement C): p. 1114-1119, DOI: https://doi.org/10.1016/j.apenergy.2013.04.072.

10.   Patel, N.S., V. Pavlík, and M. Boča, *High-Temperature Corrosion Behavior of Superalloys in Molten Salts–A Review.* Critical Reviews in Solid State and Materials Sciences, 2017. **42**(1): p. 83-97, DOI: 10.1080/10408436.2016.1243090.

11.   Calderón, A., A. Palacios, C. Barreneche, M. Segarra, C. Prieto, A. Rodriguez-Sanchez, and A.I. Fernández, *High temperature systems using solid particles as TES and HTF material: A review.* Applied Energy, 2018. **213**: p. 100-111, DOI: https://doi.org/10.1016/j.apenergy.2017.12.107.

12.   Prieto, C., P. Cooper, A.I. Fernández, and L.F. Cabeza, *Review of technology: Thermochemical energy storage for concentrated solar power plants.* Renewable and Sustainable Energy Reviews, 2016. **60**: p. 909-929, DOI: 10.1016/j.rser.2015.12.364.

13.   André, L., S. Abanades, and G. Flamant, *Screening of thermochemical systems based on solid-gas reversible reactions for high temperature solar thermal energy storage.* Renewable and Sustainable Energy Reviews, 2016. **64**(Supplement C): p. 703-715, DOI: https://doi.org/10.1016/j.rser.2016.06.043.

14.   Pardo, P., A. Deydier, Z. Anxionnaz-Minvielle, S. Rougé, M. Cabassud, and P. Cognet, *A review on high temperature thermochemical heat energy storage.* Renewable and Sustainable Energy Reviews, 2014. **32**(Supplement C): p. 591-610, DOI: https://doi.org/10.1016/j.rser.2013.12.014.

15.   Dizaji, H.B. and H. Hosseini, *A review of material screening in pure and mixed-metal oxide thermochemical energy storage (TCES) systems for concentrated solar power (CSP) applications.* Renewable and Sustainable Energy Reviews, 2018. **98**: p. 9-26, DOI: 10.1016/j.rser.2018.09.004.

16.   Benitez-Guerrero, M., J.M. Valverde, P.E. Sanchez-Jimenez, A. Perejon, and L.A. Perez-Maqueda, *Multicycle activity of natural CaCO3 minerals for thermochemical energy storage in Concentrated Solar Power plants.* Solar Energy, 2017. **153**(Supplement C): p. 188-199, DOI: https://doi.org/10.1016/j.solener.2017.05.068.

17.   Lisbona, P., A. Martínez, Y. Lara, and L.M. Romeo, *Integration of carbonate CO_2 capture cycle and coal-fired power plants. A comparative study for different sorbents.* Energy & Fuels, 2010. **24**(1): p. 728-736, DOI: 10.1021/ef900740p.

18.   Parrado, C., A. Marzo, E. Fuentealba, and A.G. Fernández, *2050 LCOE improvement using new molten salts for thermal energy storage in CSP plants.* Renewable and Sustainable Energy Reviews, 2016. **57**: p. 505-514, DOI: 10.1016/j.rser.2015.12.148.

19.   Barker, R., *The reactivity of calcium oxide towards carbon dioxide and its use for energy storage.* Journal of Applied Chemistry and Biotechnology, 1974. **24**(4-5): p. 221-227, DOI: 10.1002/jctb.2720240405.

20.   Flamant, G., D. Hernandez, C. Bonet, and J.-P. Traverse, *Experimental aspects of the thermochemical conversion of solar energy; Decarbonation of CaCO3.* Solar Energy, 1980. **24**(4): p. 385-395, DOI: https://doi.org/10.1016/0038-092X(80)90301-1.

21. Blamey, J., E.J. Anthony, J. Wang, and P.S. Fennell, *The calcium looping cycle for large-scale CO₂ capture.* Progress in Energy and Combustion Science, 2010. **36**(2): p. 260-279, DOI: 10.1016/j.pecs.2009.10.001.

22. Boot-Handford, M.E., J.C. Abanades, E.J. Anthony, M.J. Blunt, S. Brandani, N. Mac Dowell, J.R. Fernandez, M.-C. Ferrari, R. Gross, J.P. Hallett, R.S. Haszeldine, P. Heptonstall, A. Lyngfelt, Z. Makuch, E. Mangano, R.T.J. Porter, M. Pourkashanian, G.T. Rochelle, N. Shah, J.G. Yao, and P.S. Fennell, *Carbon capture and storage update.* Energy & Environmental Science, 2014. **7**(1): p. 130-189, DOI: 10.1039/C3EE42350F.

23. Borgwardt, R.H., *Calcium oxide sintering in atmospheres containing water and carbon dioxide.* Industrial & Engineering Chemistry Research, 1989. **28**(4): p. 493-500, DOI: 10.1021/ie00088a019.

24. Valverde, J.M., P.E. Sanchez-Jimenez, L.A. Perez-Maqueda, M.A.S. Quintanilla, and J. Perez-Vaquero, *Role of crystal structure on CO₂ capture by limestone derived CaO subjected to carbonation/recarbonation/calcination cycles at Ca-looping conditions.* Applied Energy, 2014. **125**: p. 264-275, DOI: 10.1016/j.apenergy.2014.03.065.

25. Valverde, J.M., P.E. Sanchez-Jimenez, and L.A. Perez-Maqueda, *Relevant influence of limestone crystallinity on CO₂ capture in the Ca-Looping technology at realistic calcination conditions.* Environmental Science & Technology, 2014. **48**(16): p. 9882-9889, DOI: 10.1021/es5014505.

26. Manovic, V. and E.J. Anthony, *Thermal activation of CaO-based sorbent and self-reactivation during CO₂ capture looping cycles.* Environmental Science & Technology, 2008. **42**(11): p. 4170-4174, DOI: 10.1021/es800152s.

27. Valverde, J.M., P.E. Sanchez-Jimenez, and L.A. Perez-Maqueda, *Role of precalcination and regeneration conditions on postcombustion CO₂ capture in the Ca-looping technology.* Applied Energy, 2014. **136**: p. 347-356, DOI: 10.1016/j.apenergy.2014.09.052.

28. Valverde, J.M., P.E. Sanchez-Jimenez, and L.A. Perez-Maqueda, *Ca-looping for postcombustion CO₂ capture: A comparative analysis on the performances of dolomite and limestone.* Applied Energy, 2015. **138**(0): p. 202-215, DOI: http://dx.doi.org/10.1016/j.apenergy.2014.10.087.

29. Erans, M., V. Manovic, and E.J. Anthony, *Calcium looping sorbents for CO2 capture.* Applied Energy, 2016. **180**(Supplement C): p. 722-742, DOI: https://doi.org/10.1016/j.apenergy.2016.07.074.

30. Kierzkowska, A.M., R. Pacciani, and C.R. Müller, *CaO-Based CO₂ sorbents: from fundamentals to the development of new, highly effective materials.* ChemSusChem, 2013. **6**(7): p. 1130-1148, DOI: 10.1002/cssc.201300178.

31. Naeem, M.A., A. Armutlulu, Q. Imtiaz, and C.R. Müller, *CaO-Based CO2 Sorbents Effectively Stabilized by Metal Oxides.* ChemPhysChem, 2017. **18**(22): p. 3280-3285, DOI: 10.1002/cphc.201700695.

32. Sanchez-Jimenez, P.E., L.A. Perez-Maqueda, and J.M. Valverde, *Nanosilica supported CaO: A regenerable and mechanically hard CO2 sorbent at Ca-looping conditions.* Applied Energy, 2014. **118**: p. 92-99, DOI: 10.1016/j.apenergy.2013.12.024.

33. Armutlulu, A., M.A. Naeem, H.-J. Liu, S.M. Kim, A. Kierzkowska, A. Fedorov, and C.R. Müller, *Multishelled CaO Microspheres Stabilized by Atomic Layer Deposition of Al2O3 for Enhanced CO2 Capture Performance.* Advanced Materials, 2017. **29**(41): p. n/a-n/a, DOI: 10.1002/adma.201702896.

34. Benitez-Guerrero, M., J.M. Valverde, A. Perejon, P.E. Sanchez-Jimenez, and L.A. Perez-Maqueda, *Low-cost Ca-based composites synthesized by biotemplate method for*

thermochemical energy storage of concentrated solar power. Applied Energy, 2018. **210**: p. 108-116, DOI: 10.1016/j.apenergy.2017.10.109.

35. Perejón, A., L.M. Romeo, Y. Lara, P. Lisbona, A. Martínez, and J.M. Valverde, *The Calcium-Looping technology for CO2 capture: On the important roles of energy integration and sorbent behavior.* Applied Energy, 2016. **162**: p. 787-807, DOI: 10.1016/j.apenergy.2015.10.121.

36. Cormos, A.-M. and A. Simon, *Assessment of CO₂ capture by calcium looping (CaL) process in a flexible power plant operation scenario.* Applied Thermal Engineering, 2015. **80**(0): p. 319-327, DOI: http://dx.doi.org/10.1016/j.applthermaleng.2015.01.059.

37. Valverde, J.M., P.E. Sanchez-Jimenez, and L.A. Perez-Maqueda, *Calcium-looping for post-combustion CO₂ capture. On the adverse effect of sorbent regeneration under CO₂.* Applied Energy, 2014. **126**(0): p. 161-171, DOI: http://dx.doi.org/10.1016/j.apenergy.2014.03.081.

38. Arias, B., G.S. Grasa, M. Alonso, and J.C. Abanades, *Post-combustion calcium looping process with a highly stable sorbent activity by recarbonation.* Energy & Environmental Science, 2012. **5**(6): p. 7353-7359, DOI: 10.1039/C2EE03008J.

39. Sarrion, B., J.M. Valverde, A. Perejon, L. Perez-Maqueda, and P.E. Sanchez-Jimenez, *On the Multicycle Activity of Natural Limestone/Dolomite for Thermochemical Energy Storage of Concentrated Solar Power.* Energy Technology, 2016: p. n/a-n/a, DOI: 10.1002/ente.201600068.

40. Chacartegui, R., A. Alovisio, C. Ortiz, J.M. Valverde, V. Verda, and J.A. Becerra, *Thermochemical energy storage of concentrated solar power by integration of the calcium looping process and a CO2 power cycle.* Applied Energy, 2016. **173**(Supplement C): p. 589-605, DOI: https://doi.org/10.1016/j.apenergy.2016.04.053.

41. Ortiz, C., M.C. Romano, J.M. Valverde, M. Binotti, and R. Chacartegui, *Process integration of Calcium-Looping thermochemical energy storage system in concentrating solar power plants.* Energy, 2018. **155**: p. 535-551, DOI: https://doi.org/10.1016/j.energy.2018.04.180.

42. Ávila-Marín, A.L., *Volumetric receivers in Solar Thermal Power Plants with Central Receiver System technology: A review.* Solar Energy, 2011. **85**(5): p. 891-910, DOI: https://doi.org/10.1016/j.solener.2011.02.002.

43. Ortiz, C., J.M. Valverde, R. Chacartegui, and L.A. Perez-Maqueda, *Carbonation of Limestone Derived CaO for Thermochemical Energy Storage: From Kinetics to Process Integration in Concentrating Solar Plants.* ACS Sustainable Chemistry & Engineering, 2018. **6**(5): p. 6404-6417, DOI: 10.1021/acssuschemeng.8b00199.

44. Ho, C.K., *A review of high-temperature particle receivers for concentrating solar power.* Applied Thermal Engineering, 2016. **109**: p. 958-969, DOI: 10.1016/j.applthermaleng.2016.04.103.

45. Koepf, E., I. Alxneit, C. Wieckert, and A. Meier, *A review of high temperature solar driven reactor technology: 25 years of experience in research and development at the Paul Scherrer Institute.* Applied Energy, 2017. **188**: p. 620-651, DOI: 10.1016/j.apenergy.2016.11.088.

46. Zsembinszki, G., A. Sole, C. Barreneche, C. Prieto, A.I. Fernández, and L.F. Cabeza, *Review of reactors with potential use in thermochemical energy storage in concentrated solar power plants.* Energies, 2018. **11**(9), DOI: 10.3390/en11092358.

47. *SOLPART project. Temperature solar-heated reactors for industrial production of reactive particulates.* http://www.solpart-project.eu [cited 10 Oct 2018.

48. Benitez-Guerrero, M., B. Sarrion, A. Perejon, P.E. Sanchez-Jimenez, L.A. Perez-Maqueda, and J. Manuel Valverde, *Large-scale high-temperature solar energy storage using natural minerals.* Solar Energy Materials and Solar Cells, 2017. **168**(Supplement C): p. 14-21, DOI: https://doi.org/10.1016/j.solmat.2017.04.013.

49.   Alvarez, D. and J.C. Abanades, *Determination of the critical product layer thickness in the reaction of CaO with CO₂.* Industrial & Engineering Chemistry Research, 2005. **44**(15): p. 5608-5615, DOI: 10.1021/ie050305s.

50.   Kim, S.M., W.-C. Liao, A.M. Kierzkowska, T. Margossian, D. Hosseini, S. Yoon, M. Broda, C. Copéret, and C.R. Müller, *In Situ XRD and Dynamic Nuclear Polarization Surface Enhanced NMR Spectroscopy Unravel the Deactivation Mechanism of CaO-Based, Ca3Al2O6-Stabilized CO2 Sorbents.* Chemistry of Materials, 2018, DOI: 10.1021/acs.chemmater.7b05034.

51.   Ma, X., Y. Li, L. Duan, E. Anthony, and H. Liu, *CO2 capture performance of calcium-based synthetic sorbent with hollow core-shell structure under calcium looping conditions.* Applied Energy, 2018. **225**: p. 402-412, DOI: https://doi.org/10.1016/j.apenergy.2018.05.008.

52.   Obermeier, J., K.G. Sakellariou, N.I. Tsongidis, D. Baciu, G. Charalambopoulou, T. Steriotis, K. Müller, G. Karagiannakis, A.G. Konstandopoulos, A. Stubos, and W. Arlt, *Material development and assessment of an energy storage concept based on the CaO-looping process.* Solar Energy, 2017. **150**: p. 298-309, DOI: https://doi.org/10.1016/j.solener.2017.04.058.

53.   Sun, X., D. Fang, L. Zhang, F. Duan, and Y. Sun, *Performance study of modified calcium magnesium acetate (MCMA) in the process of high temperature CO2 capture and the application of spent MCMA for sequential SO2 removal.* Asia-Pacific Journal of Chemical Engineering, 2017. **12**(4): p. 595-604, DOI: 10.1002/apj.2101.

54.   Oh, S.J., G.G. Choi, and J.S. Kim, *Production of acetic acid-rich bio-oils from the fast pyrolysis of biomass and synthesis of calcium magnesium acetate deicer.* Journal of Analytical and Applied Pyrolysis, 2017. **124**: p. 122-129, DOI: 10.1016/j.jaap.2017.01.032.

55.   Miranda-Pizarro, J., A. Perejón, J.M. Valverde, L.A. Pérez-Maqueda, and P.E. Sánchez-Jiménez, *CO2 capture performance of Ca-Mg acetates at realistic Calcium Looping conditions.* Fuel, 2017. **196**(Supplement C): p. 497-507, DOI: https://doi.org/10.1016/j.fuel.2017.01.119.

56.   Lu, H., E.P. Reddy, and P.G. Smirniotis, *Calcium Oxide Based Sorbents for Capture of Carbon Dioxide at High Temperatures.* Industrial & Engineering Chemistry Research, 2006. **45**(11): p. 3944-3949, DOI: 10.1021/ie051325x.

57.   de la Calle Martos, A., J.M. Valverde, P.E. Sanchez-Jimenez, A. Perejon, C. Garcia-Garrido, and L.A. Perez-Maqueda, *Effect of dolomite decomposition under CO2 on its multicycle CO2 capture behaviour under calcium looping conditions.* Physical Chemistry Chemical Physics, 2016. **18**(24): p. 16325-16336, DOI: 10.1039/C6CP01149G.

58.   Grasa, G., R. Murillo, M. Alonso, and J.C. Abanades, *Application of the random pore model to the carbonation cyclic reaction.* AIChE Journal, 2009. **55**(5): p. 1246-1255, DOI: 10.1002/aic.11746.

59.   Sanchez-Jimenez, P.E., J.M. Valverde, and L.A. Perez-Maqueda, *Multicyclic conversion of limestone at Ca-looping conditions: The role of solid-sate diffusion controlled carbonation.* Fuel, 2014. **127**: p. 131-140, DOI: 10.1016/j.fuel.2013.09.064.

60.   Sun, Z., S. Luo, P. Qi, and L.-S. Fan, *Ionic diffusion through Calcite (CaCO₃) layer during the reaction of CaO and CO₂.* Chemical Engineering Science, 2012. **81**(0): p. 164-168, DOI: http://dx.doi.org/10.1016/j.ces.2012.05.042.

61.   Valverde, J.M., P.E. Sanchez-Jimenez, and L.A. Perez-Maqueda, *Limestone calcination nearby equilibrium: kinetics, CaO crystal structure, sintering and reactivity.* Journal of Physical Chemistry C, 2015. **119**(4): p. 1623-1641, DOI: 10.1021/jp508745u.

62.   Grasa, G.S., J.C. Abanades, M. Alonso, and B. González, *Reactivity of highly cycled particles of CaO in a carbonation/calcination loop.* Chemical Engineering Journal, 2008. **137**(3): p. 561-567, DOI: https://doi.org/10.1016/j.cej.2007.05.017.
63.   Taketomo, E. and M. Fujiura, *Porous materials for concentration and separation of hydrogen or helium, and process therewith for the separation of the gas*. 1984.